EBioMedicine 2 (2015) 730–743

Contents lists available at ScienceDirect

EBioMedicine

journal homepage: www.ebiomedicine.com

Original Article

Sustained Brown Fat Stimulation and Insulin Sensitization by a Humanized Bispecific Antibody Agonist for Fibroblast Growth Factor Receptor 1/βKlotho Complex

Ganesh Kolumam [a], Mark Z. Chen [a], Raymond Tong [b], Jose Zavala-Solorio [a], Lance Kates [a], Nicholas van Bruggen [c], Jed Ross [c], Shelby K. Wyatt [c], Vineela D. Gandham [c], Richard A.D. Carano [c], Diana Ronai Dunshee [a], Ai-Luen Wu [a], Benjamin Haley [a], Keith Anderson [a], Søren Warming [a], Xin Y. Rairdan [d], Nicholas Lewin-Koh [e], Yingnan Zhang [f], Johnny Gutierrez [g], Amos Baruch [g], Thomas R. Gelzleichter [h], Dale Stevens [h], Sharmila Rajan [i], Travis W. Bainbridge [b], Jean-Michel Vernes [j], Y. Gloria Meng [j], James Ziai [k], Robert H. Soriano [a], Matthew J. Brauer [l], Yongmei Chen [m], Scott Stawicki [m], Hok Seon Kim [m], Laëtitia Comps-Agrar [j], Elizabeth Luis [b], Christoph Spiess [m], Yan Wu [m], James A. Ernst [b], Owen P. McGuinness [n], Andrew S. Peterson [a], Junichiro Sonoda [a,*]

[a] Molecular Biology, Genentech, Inc., South San Francisco, CA 94080, USA
[b] Protein Chemistry, Genentech, Inc., South San Francisco, CA 94080, USA
[c] Biomedical Imaging, Genentech, Inc., South San Francisco, CA 94080, USA
[d] Transgenic Technology, Genentech, Inc., South San Francisco, CA 94080, USA
[e] Biostatistics, Genentech, Inc., South San Francisco, CA 94080, USA
[f] Early Discovery Biochemistry, Genentech, Inc., South San Francisco, CA 94080, USA
[g] ITGR/NTA Pharmacodynamic Biomarkers, Genentech, Inc., South San Francisco, CA 94080, USA
[h] Safety Assessment, Genentech, Inc., South San Francisco, CA 94080, USA
[i] Preclinical & Translational Pharmacokinetics, Genentech, Inc., South San Francisco, CA 94080, USA
[j] Biochemical and Cellular Pharmacology, Genentech, Inc., South San Francisco, CA 94080, USA
[k] Pathology, Genentech, Inc., South San Francisco, CA 94080, USA
[l] Bioinformatics and Computational Biology, Genentech, Inc., South San Francisco, CA 94080, USA
[m] Antibody Engineering, Genentech, Inc., South San Francisco, CA 94080, USA
[n] Department of Molecular Physiology and Biophysics, Vanderbilt University School of Medicine, Nashville, TN 37232, USA

ARTICLE INFO

Article history:
Received 4 May 2015
Received in revised form 26 May 2015
Accepted 27 May 2015
Available online 30 May 2015

Keywords:
Brown adipose tissue
Therapeutic antibody
Thermogenesis
Adipose tissue browning
Humanized antibody
Adiponectin
FGF21
FGF19
FGFR1
betaKlotho
UCP1
Bispecific antibody
Insulin resistance
Obesity
Type 2 diabetes
Hepatosteatosis
NASH

ABSTRACT

Dissipating excess calories as heat through therapeutic stimulation of brown adipose tissues (BAT) has been proposed as a potential treatment for obesity-linked disorders. Here, we describe the generation of a humanized effector-less bispecific antibody that activates fibroblast growth factor receptor (FGFR) 1/βKlotho complex, a common receptor for FGF21 and FGF19. Using this molecule, we show that antibody-mediated activation of FGFR1/βKlotho complex in mice induces sustained energy expenditure in BAT, browning of white adipose tissue, weight loss, and improvements in obesity-associated metabolic derangements including insulin resistance, hyperglycemia, dyslipidemia and hepatosteatosis. In mice and cynomolgus monkeys, FGFR1/βKlotho activation increased serum high-molecular-weight adiponectin, which appears to contribute over time by enhancing the amplitude of the metabolic benefits. At the same time, insulin sensitization by FGFR1/βKlotho activation occurs even before the onset of weight loss in a manner that is independent of adiponectin. Together, selective activation of FGFR1/βKlotho complex with a long acting therapeutic antibody represents an attractive approach for the treatment of type 2 diabetes and other obesity-linked disorders through enhanced energy expenditure, insulin sensitization and induction of high-molecular-weight adiponectin.

* Corresponding author.
E-mail address: junichis@gene.com (J. Sonoda).

http://dx.doi.org/10.1016/j.ebiom.2015.05.028

1. Introduction

Chronic positive energy balance through the consumption of calorie-rich foods is common in modern society and the major driver of the obesity pandemic that has become the leading cause of disability around the world (Ng et al., 2014). Several associated metabolic derangements are linked to obesity including insulin resistance, hyperinsulinemia, hyperlipidemia, and hepatosteatosis, which often lead to severe illnesses such as type 2 diabetes, liver cirrhosis, stroke and heart disease (Shulman, 2014). Pharmacological agents that increase energy expenditure (EE) in humans exist, but all have failed so far to correct energy balance safely in obese individuals (Yen and Ewald, 2012).

Mammals possess a specialized organ known as brown adipose tissue (BAT) whose function is to maintain body temperature through non-shivering thermogenesis. BAT is characterized by high mitochondria content and expression of the thermogenic protein uncoupling protein 1 (UCP1), which enables the conversion of energy to heat upon stimulation by cold exposure (Cannon and Nedergaard, 2004). Over the last decade, it has been increasingly recognized that adult humans possess a variable amount of BAT (Nedergaard et al., 2007; Sidossis and Kajimura, 2015), and repeated cold (Yoneshiro et al., 2013) or catecholamine exposure (Cypess et al., 2015; Frontini et al., 2013; Sondergaard et al., 2015) can increase the amount and the activity of human BAT. These findings ignited an immense interest in therapeutic induction and stimulation of thermogenic brown adipocytes as a potential treatment for individuals with obesity-related metabolic defects (Sidossis and Kajimura, 2015).

Fibroblast growth factor 21 (FGF21) and its closest homologue FGF19 are two members of the FGF superfamily that have been found to stimulate BAT thermogenesis and increase EE in rodents (Coskun et al., 2008; Fu et al., 2004; Tomlinson et al., 2002; Xu et al., 2009). Supraphysiological exposure to these secreted proteins ameliorates obesity, insulin resistance, hyperlipidemia, fatty liver, and hyperglycemia (Coskun et al., 2008; Fu et al., 2004; Xu et al., 2009). In addition, FGF21 induces the emergence of UCP1-positive adipocytes in the white adipose tissue (WAT) depot, a process now termed *browning* (Fisher et al., 2012). Although clinical applications of recombinant FGF21 or FGF19 analogs are currently being investigated for the treatment of metabolic disease with some initial success (Gaich et al., 2013), studies in rodents suggest potential risks for adverse effects in chronic treatment. For example, transgenic overproduction of FGF21 leads to stunted growth, bone loss, female infertility, and an increase in serum glucocorticoid (Bookout et al., 2013; Inagaki et al., 2008; Owen et al., 2013; Wei et al., 2012). Transgenic overproduction of FGF19 does not elicit the same safety issues as FGF21, but instead leads to hepatocellular carcinogenesis via activation of FGF Receptor (FGFR) 4 (French et al., 2012; Fu et al., 2004; Tomlinson et al., 2002). The pharmacological profiles of these two related molecules suggest that selective activation of a common receptor may provide beneficial metabolic effects without the molecule-specific long-term side effects.

Of the seven primary FGFR isoforms (1b, 1c, 2b, 2c, 3b, 3c, and 4) expressed in mammals, both FGF19 and FGF21 can activate three of these isoforms (1c, 2c and 3c) when bound to their obligate coreceptor βKlotho (KLB) to transduce the mitogen-activated-protein-kinase (MAPK) signaling cascade (Kurosu et al., 2007). KLB is expressed in select tissues, most abundantly, in liver, pancreas and adipose tissues (Fon Tacer et al., 2010). Studies using tissue-specific gene knockout in mice have emphasized the critical role in mediating the metabolic actions of FGF21 of FGFR1 and KLB in adipose tissue (Adams et al., 2012; Ding et al., 2012; Foltz et al., 2012) and of KLB in the central nervous system (Owen et al., 2014). Although non-FGF-based agonists for FGFR1/KLB complex that induce weight loss in obese monkeys have been described (Foltz et al., 2012; Smith et al., 2013), the mechanistic basis underlying the observed weight loss remains largely unclear. Thus, it is not known whether the activation of FGFR1/KLB complex is sufficient to drive induction of EE and WAT browning. In addition, FGF21 increases circulating adiponectin levels in rodent and primate species (Gaich et al., 2013; Holland et al., 2013; Kharitonenkov et al., 2007; Lin et al., 2013), but at least in one case, an FGFR1/KLB agonist antibody did not affect plasma adiponectin levels despite the observed weight loss (Foltz et al., 2012).

Here we describe the generation of a humanized bispecific anti-FGFR1/KLB antibody that acts as a selective agonist for FGFR1/KLB receptor complex. Using this molecule, we demonstrate that activation of FGFR1/KLB complex in mice leads to sustained stimulation of thermogenic activity in BAT and induction of WAT browning, resulting in the efficacious amelioration of obesity, insulin resistance and associated metabolic defects. Antibody-mediated activation of FGFR1/KLB complex was also found sufficient to increase adiponectin levels in both mice and cynomolgus monkeys.

2. Materials and Methods

2.1. Research Ethics

All animal studies were conducted in accordance with the Guide for the Care and Use of Laboratory Animals, published by the National Institutes of Health (NIH) (NIH Publication 8523, revised 1985). The Institutional Animal Care and Use Committee (IACUC) at Genentech or Vanderbilt University reviewed and approved all animal protocols.

2.2. Isolation and Characterization of Bispecific Anti-FGFR1/KLB Ab

Isolation of phage derived anti-FGFR1 antibodies was described previously (Wu et al., 2011a). Anti-KLB antibodies were generated by immunizing Balb/c female mice with HEK293 cells stably expressing human (h)FGFR1c and hKLB proteins. Each hybridoma line was selected by FACS using HEK293 cells expressing hKLB, hFGFR1c, or both, and the cDNA encoding each antibody heavy chain and light chain was cloned into expression vectors. The initial screening of bispecific antibody pairs was conducted using crudely purified antibodies expressed in HEK293T cells co-transfected with a mixture of four expression vectors encoding the heavy and light chains of anti-FGFR1 and anti-KLB IgG as described in Supplemental Materials and Methods. For production of pure and homogenenous bispecific antibodies, anti-FGFR1 and anti-KLB arms with the knob or the hole mutation were separately purified from transiently or stably transfected CHO cell culture supernatant by affinity purification using Protein A column, and then subjected to an annealing protocol as previously described (Shatz et al., 2013).

2.3. Mouse Strains

Mice were purchased from Jackson Laboratory or Taconic. *db*/*db* mice in C57BLKS/J background were females. Homozygous *Klb*-deficient (KO) mice in C57BL/6 background were semi-lethal, and crossed with Balb/c mice; male mice used were in mixed background. Other mice were all C57BL/6 males or males in C57BL/6 background. To generate *Klb* KO mice, a *Klb*-specific Zinc Finger Nuclease (ZFN) pair was obtained from Sigma-Aldrich and used for pronuclear microinjection according to established methods. The ZFN pair targets the following *Klb* sequence in the mouse genome (cut site in small letters), and the KO mice lack one base-pair (g in bold) causing a frameshift after the second amino acid encoding the mature KLB protein: GTTACCGGCTTCtccg**g**aGACGGGAAAGCAATATGG.

2.4. Mouse Studies

All the mice were maintained in a pathogen-free animal facility under standard 12 h light/12 h dark cycle with access to normal chow (Labdiet 5010) or high fat diet (HFD; Harlan Teklad TD.06414, 58.4% calories from fat) and water ad libitum. All the mouse experiments were

conducted at 21 °C, unless otherwise indicated. All the mice used for intervention studies were around 2–6 months old and were randomized into groups based on body weight, blood glucose levels, and/or specific parameters being examined at the pre-dose state. For glucose tolerance test (GTT), mice were fasted overnight, and intraperitoneally (i.p.) injected with 2 g/kg glucose solution. For insulin tolerance test (ITT), mice were fasted for 4 h, and i.p. injected with 1 U/kg human insulin solution (Humulin R, Eli Lilly). Hyperinsulinemic euglycemic clamp experiments were conducted at the Vanderbilt University Mouse Metabolic Phenotyping Center using standard procedures (Ayala et al., 2006). Details of mouse studies can also be found in Supplemental Materials and Methods.

2.5. Metabolic Measurements

Oxymax system (Columbus Instruments) was used to measure oxygen consumption (VO_2), carbon dioxide production (VCO_2) and locomotor activity. After acclimation to the cages, mice were randomized into groups based on body weight and baseline metabolic parameters. The following equations were used to calculate EE and the respiratory quotient (RQ). $EE = VO_2 \times (3.815 + 1.232 \times RQ)$. $RQ = VO_2 / VCO_2$. For core body temperature monitoring, TA-F10 transmitter (DSI) was surgically implanted into peritoneal cavity. Core body temperature and activity were monitored using DSI Implantable Telemetry System. After recovery from the surgery, mice were randomized into groups based on body weight and basal core body temperature.

2.6. Monkey Study

The study was conducted with drug-naive healthy male cynomolgus monkeys, aged 2–3 years at Covance Laboratories Inc., according to a written study protocol and facility standard operating procedures in strict compliance with national legal regulations on animal welfare and accepted animal welfare standards. Three animals per group were chosen as the minimum number of animals necessary for assessment of inter-animal variability. Animals were randomized into groups based on the basal body weight. Serum samples were collected after a minimum of 9 h fast at baseline and at different time points post dose.

2.7. Gene Expression Analysis

For *UCP1* mRNA analysis in human primary adipocytes, total RNA was used to synthesize cDNA using SuperScript VILO cDNA Synthesis Kit (ABI). For qPCR, samples were run in triplicate in the ViiA 7 Real-Time PCR instrument (ABI). The Applied Biosystems predesigned Taqman Gene Expression Assay probe used was UCP1 (Hs01027785_m1). For each sample, mRNA abundance was normalized to the amount of TBP (Hs00427620_m1) and SDHA (Hs00188166_m1) transcripts. For tissue RNA microarray analysis, total RNA (N = 5 per group) was labeled and hybridized to Affymetrix mouse genome 430 2.0 arrays. Expression intensity for each probe set was calculated and heatmap generated using ExpressionPlot application suit (Friedman and Maniatis, 2011). Data are available at the NCBI (GEO accession number GSE68152).

2.8. Western Blot

Tissue extracts were generated by homogenizing freshly isolated tissues in T-PER Tissue Protein Extraction Reagent (Pierce) containing protease and phosphatase inhibitor tablets (Roche), and used for Western blot analysis by standard methods. Cell extracts from differentiated human primary adipocytes were generated by lysing cells in 2× LDS buffer (Invitrogen) containing protease and phosphatase inhibitor tablets (Roche). Samples were then sonicated and used for Western blot analysis by standard methods. Antibodies used for western blot analysis were from Cell Signaling Technology: pFRS2a (T196) (#3864), pMEK1/2 (S217/221) (#9154), MEK (#9126), pERK1/2 (T202/204) (#4370), ERK1/2 (#4695), HSP90 (#4874), β-Actin (#5125), from abcam: UCP1 (ab10983), or from R&D Systems: KLB (AF2619). Anti-FGFR1 D1 antibody (clone 14B6) was generated by immunizing Balb/c female mice with HEK293 cells stably expressing hFGFR1c and hKLB proteins.

2.9. In Vitro Cell Culture Experiments

Cell culture and radioligand cell binding assay were performed using standard methods as described in Supplemental Materials and Methods.

2.10. Surface Plasmon Resonance (SPR)

FGFR1–KLB–bFKB1 interaction was studied by SPR measurements on a ProteOn XPR36 instrument (Bio-Rad) at 25 °C. FGFR1–ECD (extra-cellular domain) protein (20 μg per ml) at pH 4.5 was immobilized at surface density (1000 RU) on an activated ProteOn GLC sensor chip using standard amine coupling procedures as described by the manufacturer. bFKB1 or 1:1 mixtures of bFKB1 and KLB–ECD were injected in PBS containing 0.005% v/v Tween-20, 0.3 M NaCl (pH 7.4) at a flow rate of 80 μl per min and sensorgrams for association and disassociation phases were recorded. Analytes were injected for 5 min and allowed to disassociate for 10 min. Data was referenced with interspots, processed, and disassociation constants measured with the ProteOn Manager software (version 3.0, Bio-Rad). bFKB1–KLB–FGF interaction was studied by biolayer interferometry (BLI) measurements on an Octet Red instrument (ForteBio) at 25 °C. bFKB1 (20 μg per ml) at pH 4.5 was immobilized on activated amine reactive biosensor tips as described by the manufacturer. KLB–ECD (20 μg per ml) in PBS containing 0.005% v/v Tween-20, 0.3 M NaCl (pH 7.4) was captured onto the same biosensor tips and measured with human FGF21 (R&D Systems) in the same buffer. Qualitative data was processed with the data acquisition software (ForteBio).

2.11. Cell-surface Time-resolved Fluorescence Resonance Energy Transfer (TR-FRET)

COS7 cells were co-transfected to express SNAP-tagged hFGFR1c and untagged hKLB and seeded in a white bottom 96-well plate (Costar) at 100,000 cells per well. Transfected cells were labeled 24 h post-transfection with 100 nM of donor-conjugated benzyl-guanine SNAP-Lumi4-Tb (Cisbio) and 1 μM of acceptor-conjugated benzyl-guanine SNAP-Alexa647 (NEB) for 1 h at 37 °C, 5% CO2. After three washes, the Lumi4-Tb emission and the TR-FRET signal were recorded at 620 nm and 665 nm, respectively, for 400 μs after a 60 μs delay following laser excitation at 343 nm using a Safire2 plate reader (Tecan) at t = 0 and t = 15 min after ligand addition. FRET intensity was then calculated as: (signal at 665 nm from cells labeled with SNAP-donor and SNAP-acceptor) − (signal at 665 nm from the same batch of transfected cells labeled with SNAP-donor and non labeled SNAP). The results were shown as FRET ratio = FRET intensity at 665 nm divided by the donor emission at 620 nm. In each of the replicated experiments, relative TR-FRET ratio was calculated, and used to generate means ± SEM values. More detailed description of the experimental condition will be described elsewhere (unpublished data; authors).

2.12. Statistics

Unpaired student's t-test (two-tailed) or one-way ANOVA with post-hoc Dunnett's test was used for statistical analysis to compare treatment groups. For energy expenditure and core body temperature results, the mean value was calculated for each mouse for each of the indicated durations, and the values were used to calculate statistical significance between groups. A p value <0.05 was considered statistically significant. "*ns*" stands for no significance. All the values were presented as means ± SEM unless otherwise noted. Statistical methods used for core body temperature analysis shown in Fig. 5D is described in Supplemental Materials and Methods.

2.13. Blinding

The investigators were not blinded to group assignment and outcome assessment.

2.14. Funding

All work was funded by Genentech, Inc.

3. Results

3.1. Identification of bFKB1, an FGFR1-selective FGF21 Mimetic Antibody

We previously reported the discovery of a unique anti-FGFR1 agonist antibody termed R1MAb1 that induces robust FGF21-like anti-diabetic effects in obese mice (Wu et al., 2011a). One obstacle in the development of this molecule as a therapeutic agent is that FGFR1 is expressed in a wide range of tissues, and as a result, R1MAb1 induced unintended side effects such as hypophosphatemia and hypophagia in mice (Wu et al., 2011a, 2013). This led us to the idea of conjoining an anti-FGFR1 Fab fragment to an anti-KLB Fab fragment as a bispecific antibody to generate a KLB-dependent FGFR1 agonist (Fig. 1A). A weak agonistic activity of R1MAb1 as a monomeric Fab fragment (Fig. S1A) suggested that a bispecific antibody could function in a manner that has been previously proposed for FGF21. FGF21 activates FGFRs only when recruited to the FGFR/KLB complex through its C-terminal KLB-binding tail, while the determinants for FGFR-specificity reside in its N-terminal region, which likely binds to FGFRs via a low affinity interaction (Fig. 1B) (Micanovic et al., 2009; Yie et al., 2009). To minimize KLB-independent FGFR1 activation and interference of endogenous FGF/FGFR1 interactions, the screen included a previously undescribed anti-FGFR1, R1MAb3, which shares a common epitope with R1MAb1, but exhibits no agonistic activity as a Fab fragment due to low affinity (Fig. S1B–G). Various combinations of anti-KLB antibodies and anti-FGFR1 antibodies were tested for FGFR1 and KLB-dependent MAPK activation in HEK293T cells using a GAL–ELK1 based luciferase assay (Fig. S2A and B). Additional engineering efforts ultimately yielded a bispecific effector-less humanized IgG1 molecule, and closely related framework variants with comparable in vitro activity (Figs. S2A, S2C, and S3A), henceforth referred to as bFKB1 for simplicity. The bFKB1 framework is composed of the aforementioned R1MAb3 (Kd > 300 nM) and KLBmAb1 — a hybridoma-derived high affinity anti-KLB antibody (Kd = 6.6 nM) that binds to the C-terminal portion of the KLB ECD (Fig. S3).

Employing the aforementioned luciferase assay in HEK293T cells engineered to lack *FGFR1* gene (Fig. 1C) or L6 cells lacking any endogenous FGFR (Fig. 1D), we found bFKB1 induced luciferase activity only when cells expressed both FGFR1c and KLB. Thus, bFKB1 acts as a highly selective KLB-dependent FGFR1c agonist. In contrast, hFGF21 and hFGF19 could also signal via alternate FGFRs as previously reported (Fig. 1D) (Kurosu et al., 2007). In human primary adipocytes differentiated in vitro, bFKB1 induced phosphorylation of MAPK signaling intermediates (Figs. 1E and S2C) and *UCP1* mRNA expression comparable to FGF21 (Fig. 1F).

In addition, utilizing cell-surface time-resolved fluorescence resonance energy transfer (TR-FRET) technology, we found that both bFKB1 and FGF21 enhance dimerization of FGFR1c when KLB is also present on the cell surface (Fig. 2A). Furthermore, bFKB1 stabilizes the interaction between recombinant FGFR1c–ECD and KLB–ECD proteins as previously observed for FGF21 (Fig. 2B) (Yie et al., 2012). Despite these similarities to FGF21, the bFKB1 epitope on KLB appears to differ from the binding site for FGF21 or FGF19; bFKB1 does not compete with either FGF molecule for KLB binding (Fig. 2C), and ultimately does not block the ability of FGF19 to activate MAPK signaling in hepatoma cells (Fig. 2D). These results collectively establish bFKB1 as an FGFR1/KLB-selective agonist.

3.2. bFKB1 Induces Weight Loss and BAT Thermogenesis in Obese Mice

The activity of bFKB1 on the murine receptor complex (Figs. 1C and S3A) allowed us to test its effects in vivo in mouse models of obesity and insulin resistance. bFKB1 administered i.p. lowered blood glucose levels dramatically without affecting food intake or body weight in leptin receptor deficient *db/db* mice (Fig. 3A). Lean C57BL/6 mice treated with bFKB1 also showed reduced blood glucose, but did not become hypoglycemic (Fig. 3A). High fat diet-fed (Diet Induced Obesity, DIO) mice injected with bFKB1 showed significant weight loss and blood glucose reduction (Fig. 3B), an improvement in glucose tolerance (Fig. 3C), and reductions in hepatic and serum lipids, and serum insulin (Fig. 3D) as expected from FGF21- and FGF19-like activity.

Previous studies with pharmacological doses of FGF19 or FGF21 have shown increased EE in obese mice (Coskun et al., 2008; Fu et al., 2004; Xu et al., 2009), however, the identity of FGFRs that mediate this effect has not been clearly defined. We found that single bFKB1 injection into DIO or lean mice at normal room temperature (21 °C) led to significant increase in the rate of O_2 consumption (VO_2), CO_2 production (VCO_2) and EE per injected animal without significant change in activity count (Figs. 4A–C, S4A–B). The increase in EE was sustained even when the cage temperature was elevated to thermoneutrality (30 °C) (Fig. 4B–C). In addition, a sustained increase in EE (~29 days) was observed when DIO mice pre-acclimated at thermoneutrality for 4 weeks was injected once with bFKB1 (Fig. 4D). Interestingly, the observed 15–46% increase in EE at subthermoneutrality did not accompany significant alteration in the relative rate of CO_2 production and VO_2 consumption or the respiratory quotients ($RQ = VCO_2 / VO_2$) (Fig. 4A–B). A similar increase in EE without change in RQ was elicited by continuously infusing FGF21 into DIO mice, consistent with some of the previous reports (Fig. S4C) (Xu et al., 2009). In contrast, continuous infusion with β_3-specific adrenoceptor agonist CL-316,243 induced an acute and transient increase in EE and reduction in RQ as anticipated, indicating a shift from carbohydrate oxidation to fat oxidation (Fig. S4D).

Several lines of evidence indicated that BAT stimulation plays a critical role in the increase in EE by bFKB1. First, bFKB1 injection increased uptake of ^{18}F-Fludeoxyglucose (FDG) specifically into the interscapular BAT tissue (iBAT) in mice fasted overnight (hence under a non-insulin-stimulated state), indicative of heightened energy demand (Fig. 5A). Second, single bFKB1 injection induced UCP1 protein expression in inguinal WAT (ingWAT), indicative of WAT browning (Fig. 5B). Third, using an implanted telemetry transmitter, we observed an increase in resting core body temperature after a single bFKB1 injection that lasted for ≥26 days before gradually returning to baseline (Fig. 5C–D). Although bFKB1 increased energy expenditure throughout the day (Fig. 4A–B), the peak core body temperature in bFKB1-treated mice did not increase significantly above that in control mice even when the cage temperature was shifted to thermoneutrality (Fig. 5C and E). Thus, bFKB1 injection did not interfere with the ability of mice to dissipate extra heat as necessary. Also, these observations suggest that the observed BAT activation is the primary cause of the core body temperature change, and is not secondary to the altered thermogenic needs. Finally, the gene expression signature in iBAT of bFKB1-treated or FGF21-treated mice was consistent with FGFR activation (*Spry4*, *Dusp4*, *Dusp6*, etc.) and thermogenic response (*Ucp1*, *Dio2*, *Elovl3*, *Ppargc1a*, *Bmp8b*, etc.) (Fig. 5F).

3.3. The Role of Adiponectin in the Metabolic Action of bFKB1

In addition to stimulating BAT, FGF21 has been reported to increase serum adiponectin in mice, monkeys, and humans (Gaich et al., 2013; Holland et al., 2013; Kharitonenkov et al., 2007; Lin et al., 2013). Recent studies have highlighted the role played by adiponectin in the metabolic action of FGF21 in mice (Holland et al., 2013; Lin et al., 2013). As anticipated, a single injection of bFKB1 into DIO mice (Fig. 6A) or lean

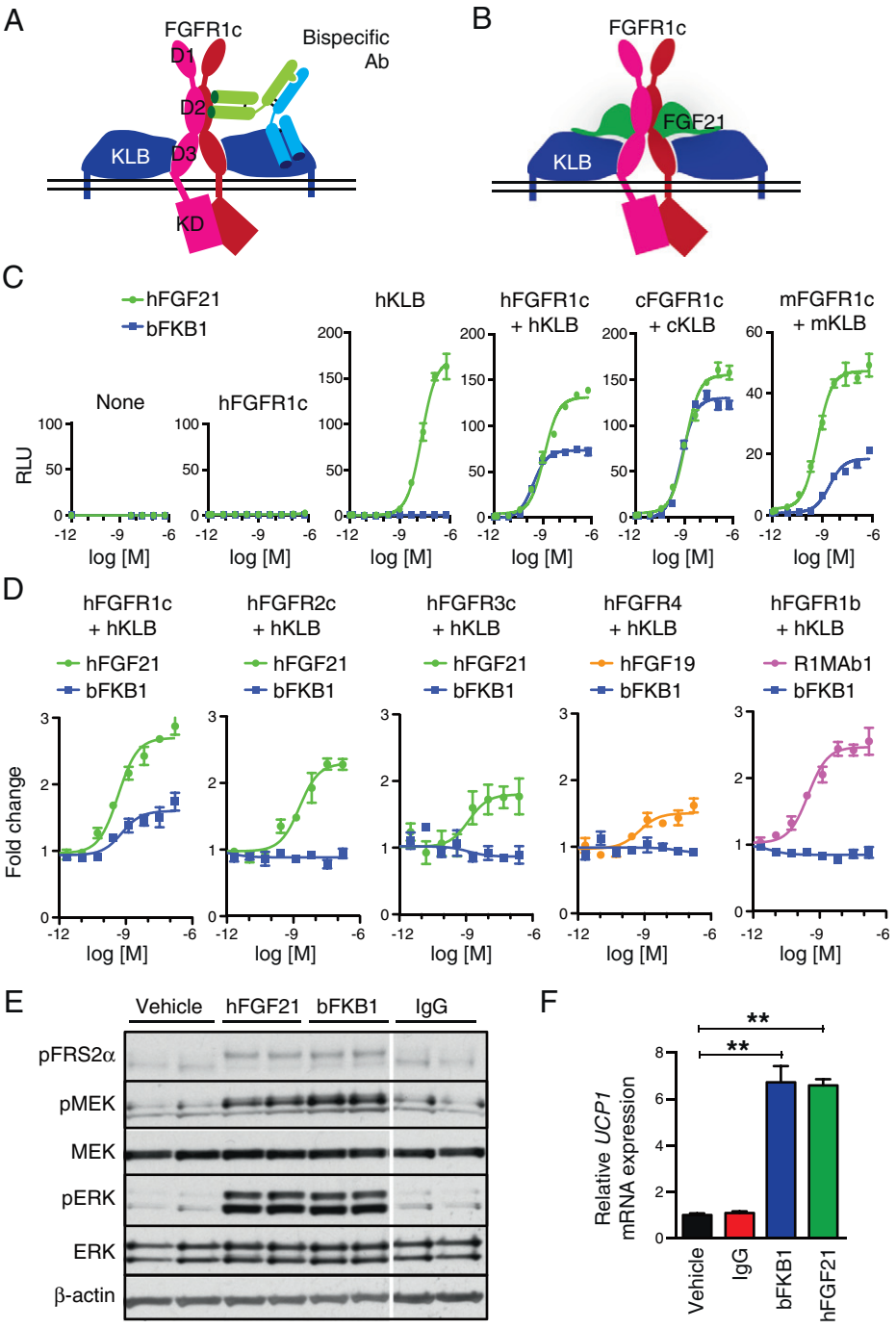

Fig. 1. Selective activation of FGFR1c/KLB complex by bFKB1 (A) A proposed model for FGFR1c–KLB–bispecific Ab (bFKB1) complex formation for signal activation. D1, D2 and D3 denote each of the Immunoglobulin-like domains in FGFR1 extra cellular domain (ECD). KD: kinase domain. (B) A predicted model for FGFR1c–KLB–FGF21 complex formation for signal activation. (C) GAL–ELK1 luciferase assay of human FGF21 and bFKB1 activity using *FGFR1*–KO HEK293T cells generated by CRISPR/Cas9-mediated genome editing. Cells were transfected to express indicated receptors. h: human, c: cynomolgus monkey, and m: murine. Mean relative luciferase unit (RLU) ± SEM is shown. (D) GAL–ELK1 luciferase assay in L6 cells. Cells were co-transfected to express indicated receptors. Transfected cells were incubated with various concentrations of bFKB1, hFGF21, hFGF19 or R1MAb1. Mean fold change ± SEM in RLU is shown. (E) Western blot analysis of primary human adipocytes treated with indicated protein (hFGF21 (100 nM) or IgG (33 nM)) for 1 h. Each treatment was performed in duplicate. (F) Expression of *UCP1* mRNA in primary human adipocytes treated with indicated protein at 30 nM for 48 h. N = 3. $p < 0.005$ (**). Data are presented as mean fold over vehicle control ± SEM.

cynomolgus monkeys (Fig. 6B) led to an increase in serum high molecular weight (HMW) adiponectin levels with associated weight loss.

The contribution of adiponectin was tested by injecting bFKB1 into wild type (WT) and *Adiponectin* (*Adipoq*) KO mice on HFD. *Adipoq* KO mice exhibited a robust response in elevating EE (20.9% increase in KO mice vs 25.3% increase in WT mice) and reduction of body weight and hepatic triglyceride levels upon bFKB1 injection (Fig. 6C and D). An improvement in insulin tolerance, serum insulin, and hepatic triglyceride levels were also observed in KO mice, however the responses were not as robust as in WT mice (Fig. 6D). Improvements in glucose tolerance, fasting blood glucose and serum triglyceride and cholesterol levels reached statistical significance only in WT mice.

We next used the hyperinsulinemic–euglycemic clamp to study the effect of bFKB1 injection on the insulin sensitivity in WT and *Adipoq* KO mice on HFD. The clamp experiment was conducted on day 3 after antibody injection, before the onset of weight loss (Fig. 7A). On the day of

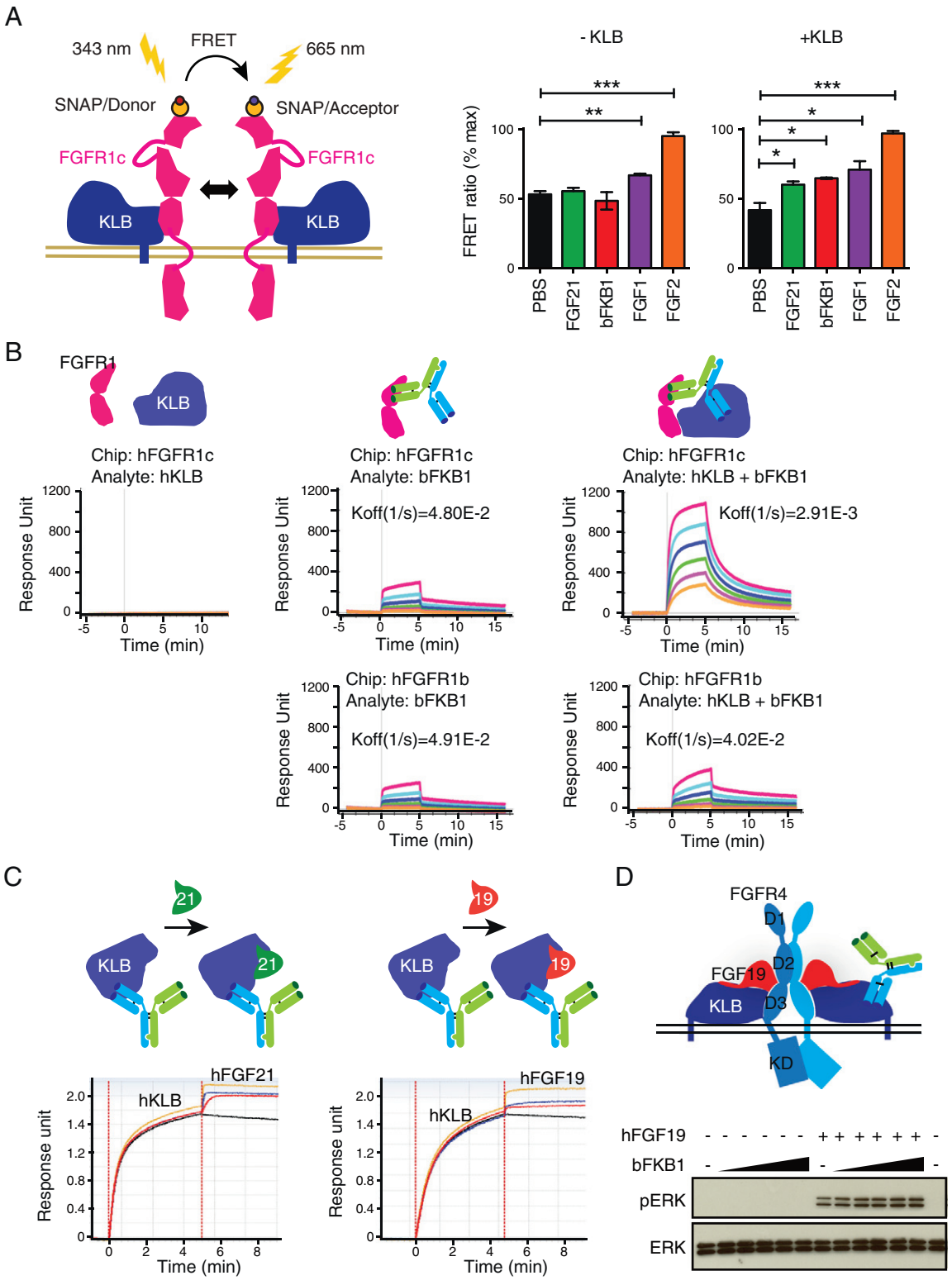

Fig. 2. Interaction between bFKB1 and FGFR1/KLB complex (A) Schematic representation of the TR-FRET experiment (left) and normalized TR-FRET ratio on COS7 cells expressing labeled SNAP-tagged hFGFR1c protein with or without untagged hKLB measured at 15 min after addition of indicated ligands (right). bFKB1, hFGF21, hFGF1 and hFGF2 were used at 67 nM, 50 nM, 62.5 nM, 125 nM, respectively. The data represents TR-FRET intensity at 665 nm divided by the donor emission at 620 nm (FRET ratio), and mean ± SEM of three independent experiments. N = 3. $p < 0.05$ (*), <0.01 (**), <0.0001 (***). (B) Evidence for a ternary complex formation by bFKB1, hFGFR1–ECD, and hKLB–ECD by SPR. hFGFR1–ECD–Fc fusion protein was immobilized on the chip, and binding of bFKB1 or preformed bFKB1/hKLB complex at 6.25, 12.5, 25, 50, 100, and 200 nM was analyzed. To generate preformed bFKB1/hKLB complex, bFKB1 and recombinant hKLB–ECD protein was preincubated at 1:1 ratio. Note the dissociation rate was slower with bFKB1/hKLB complex than with bFKB1 alone, but only when hFGFR1c, but not hFGFR1b, was captured on the chip. (C) Binding of hFGF21 and hFGF19 to bFKB1/hKLB complex by SPR. bFKB1 was captured on the chip, and hKLB–ECD protein and FGF protein (at 0.2, 0.8, or 2 μM) were sequentially injected as indicated by schematic diagram above. (D) Western blot to monitor ERK phosphorylation in H4IIE hepatoma cells. Note that bFKB1 did not block activity of hFGF19 to induce ERK phosphorylation as schematically shown on top.

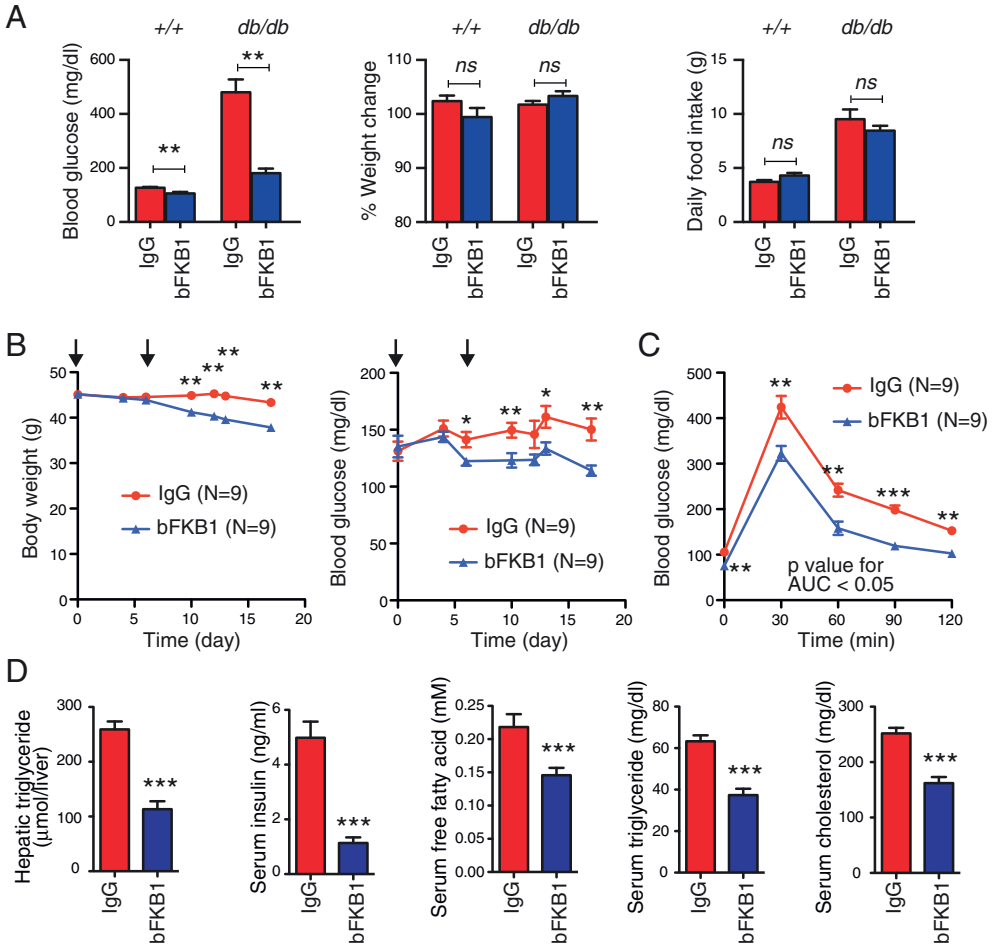

Fig. 3. Metabolic improvements in obese mice by bFKB1 (A) Blood glucose levels (day 7), % body weight change (days 0–7) and daily food intake (days 0–3) of lean (+/+) and *db/db* mice after a single i.p. injection of bFKB1 or control IgG at 3 mg/kg (mpk) (+/+) or 5 mpk (*db/db*). N = 7–8 mice per group. Pre-dose body weight was 25.8 ± 0.4 (lean, IgG), 25.9 ± 0.5 (lean, bFKB1), 39.7 ± 0.7 (*db/db*, IgG) and 39.8 ± 1.1 (*db/db*, bFKB1) g. (B) Body weight and blood glucose levels of DIO mice received i.p. injection of indicated IgG at 3 mpk on days 0 and 6 (arrows). (C) Glucose tolerance test with the same mice used in (b) on day 14. (D) Hepatic triglycerides, and serum parameters in the same mice shown in (b–c) on day 17. N = 9 mice per group. $p < 0.05$ (*), <0.005 (**), <0.0001 (***) vs control. Data are mean ± SEM.

the clamp, bFKB1-treated mice exhibited lowered fasting blood glucose at baseline and elevated glucose infusion rate required to maintain euglycemia in the face of a constant insulin infusion (96% increase in WT mice and 152% increase in *Adipoq* KO mice) (Fig. 7B). During the insulin-stimulated period, bFKB1-treated mice, irrespective of *Adipoq* genotype, exhibited higher rates of whole body glucose utilization (Fig. 7C) and glucose uptake (Rg) in multiple tissues (Fig. 7D) compared to control IgG-treated mice. Thus, bFKB1 increased insulin sensitivity (i.e. leftward shift of curve in Fig. 7C) even in the absence of adiponectin. In this experiment, bFKB1 treatment did not amplify absolute suppression of endogenous glucose production (Fig. 7E).

To determine the effect of bFKB1 treatment at a later time point, the clamp experiment was repeated just with WT DIO mice. This time the clamp experiment was conducted 5 days after the antibody injection, again before the onset of weight loss (Fig. 7F). Like the previous experiment, bFKB1-treated mice improved fasting blood glucose at the baseline (Fig. 7G), the steady state glucose infusion rate (Fig. 7G), the rate of whole body glucose utilization (Fig. 7H), and the tissue glucose uptake (Fig. 7I). In this experiment, bFKB1 enhanced hepatic insulin sensitivity and insulin suppression of endogenous glucose production (Fig. 7J).

3.4. Target Specificity and Safety Profile of bFKB1

KLB-dependency of bFKB1 in vivo was tested in *Klb*-deficient mice (Fig. 8A). As expected, *Klb* deficient DIO mice were refractory to bFKB1 as measured by energy expenditure (Fig. 8B) and glucose tolerance (Fig. 8C). In addition, unlike anti-FGFR1 R1MAb1 that alters the levels of serum FGF23 and phosphorus by activating FGFR1 in bone and kidney (Wu et al., 2011a, 2013), bFKB1 did not affect these serum parameters, indicating the absence of KLB-independent FGFR1 agonism or antagonism (Fig. 8D). Furthermore, consistent with KLB- and FGFR1-dependent mechanism, bFKB1 induced acute ERK and MEK phosphorylation in adipose tissues and pancreas, which express high levels of both KLB and FGFR1, but not in the liver where FGFR1c expression is much lower than that in adipose tissues (Fig. 8E) (Fon Tacer et al., 2010). In comparison, FGF21 induced ERK and MEK phosphorylation even in the liver, presumably through an alternate FGFR/KLB complex. These results support the liver-sparing nature of bFKB1 and the absolute requirement of the FGFR1/KLB coreceptor complex in the pharmacological action of bFKB1 in vivo.

The receptor specificity of bFKB1 and previously described low brain penetrance of IgG molecules (Yu et al., 2011) predict an altered safety profile of bFKB1 compared with FGF21 or 19. Chronic bFKB1 treatment of DIO mice for 6 weeks improved metabolic parameters as anticipated, but did not result in the deterioration of tibial trabecular and femoral cortical bones based on micro-computed tomography (µCT) (Fig. S5A). Previous studies have reported pharmacological doses of FGF19 induce hepatic cell proliferation (French et al., 2012; Wu et al., 2011b); however chronic bFKB1 treatment of DIO mice for 8 weeks not only did not trigger an increase in cell proliferation but reduced the number of proliferating cells in the liver to the level of lean mice as measured by the number of bromodeoxyuridine positive nuclei (Fig. S5B). Moreover,

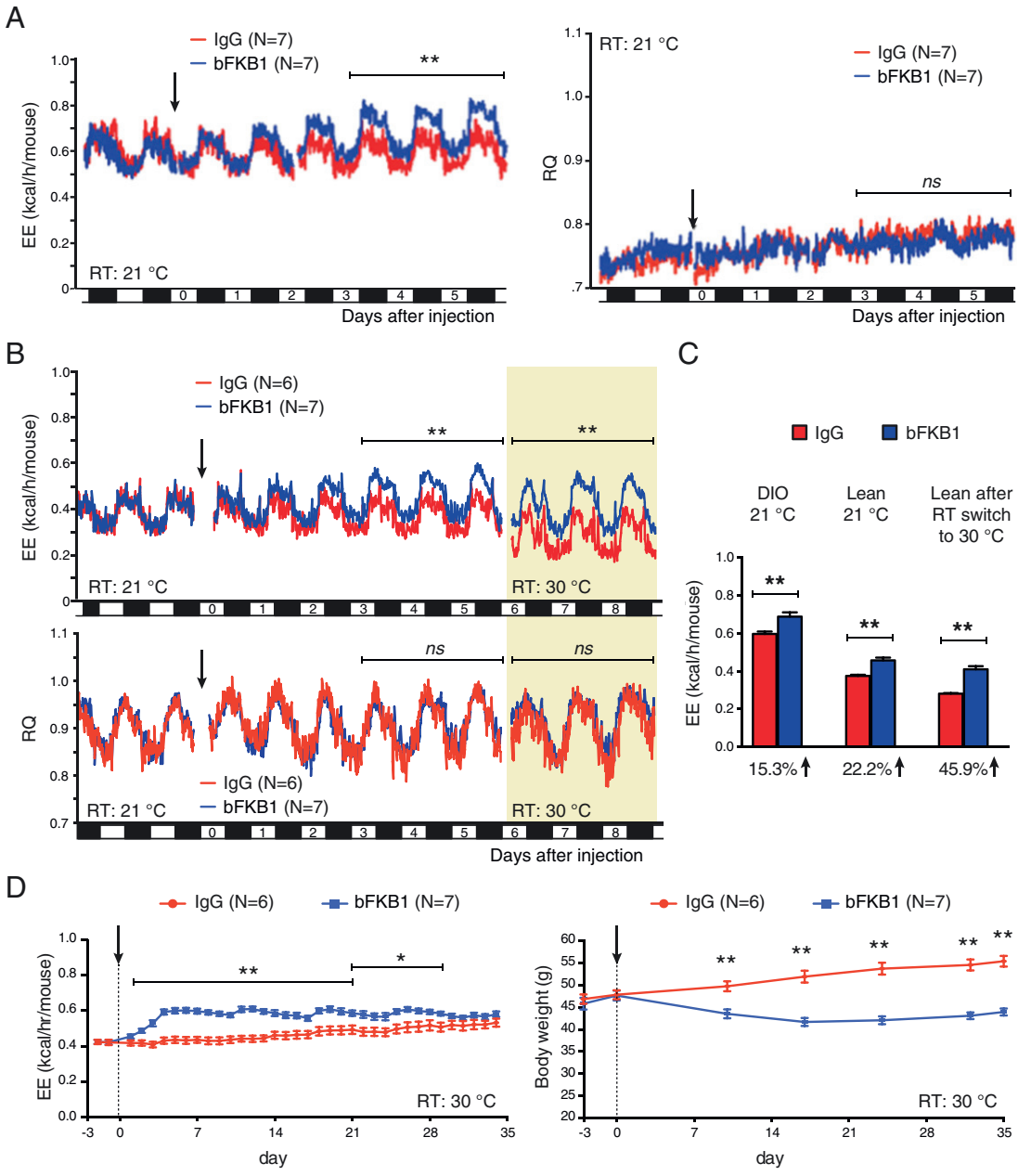

Fig. 4. Sustained induction of EE by FKB1 without altering RQ (A) Mean EE and RQ values of DIO mice received single i.p. injection of 10 mpk IgG at the indicated time (arrow). (B) Mean EE and RQ values of lean mice received single i.p. injection of 10 mpk IgG at the indicated time (arrow). Mice were maintained at 21 °C, then cage temperature was shifted to thermoneutrality (30 °C) after 6 days post IgG injection. (C) Mean EE values ± SEM in indirect calorimetry shown in (A) and (B). Mean fold increase value is shown under the graphs. (D) Daily mean EE values ± SEM per mouse (left) and body weight (right) of DIO mice received single i.p. injection of 10 mpk IgG at the indicated time (arrow). Mice were pre-acclimated at 30 °C for 4 weeks prior to the injection and then maintained at 30 °C throughout the experiment. Error bars omitted in (A) and (B) for clarity. $p < 0.05$ (*), <0.005 (**) vs control.

bFKB1 treatment did not significantly increase serum corticosterone levels above control in DIO mice (Fig. S5C). Finally, bFKB1 increased phospho-ERK signal in pancreas as expected, but not in various brain sections including circumventricular organs (Fig. S5D). Although further investigation is required to establish the site of action and the safety profile of this molecule, the available data suggests that selective activation of FGFR1/KLB complex may provide metabolic benefits without overtly compromising the safety of individuals.

4. Discussion

Recombinant monoclonal antibodies are a powerful therapeutic modality as they provide excellent target selectivity, pharmacokinetic profile, and other properties vital for pharmaceutical agents (Chan and Carter, 2010). While monoclonal antibodies only engage a single antigen, in recent years engineering efforts achieved success in creating bispecific antibodies from two independent antibodies, providing the opportunity for novel modes of action (Spiess et al., 2013). Applying this innovative technology, we generated a humanized antibody molecule bFKB1 that specifically activates the FGFR1/KLB complex both in vitro and in vivo. Overall, the observed metabolic phenotypes induced by a single bFKB1 administration in mice and monkeys are remarkably similar to what has been observed with continuous infusion or repeated administrations of FGF21 or its analogs. However, bFKB1 differs mechanistically from FGF21 in receptor selectivity. Together with KLB, FGF21 activates FGFR1c, 2c and 3c, while bFKB1 activates

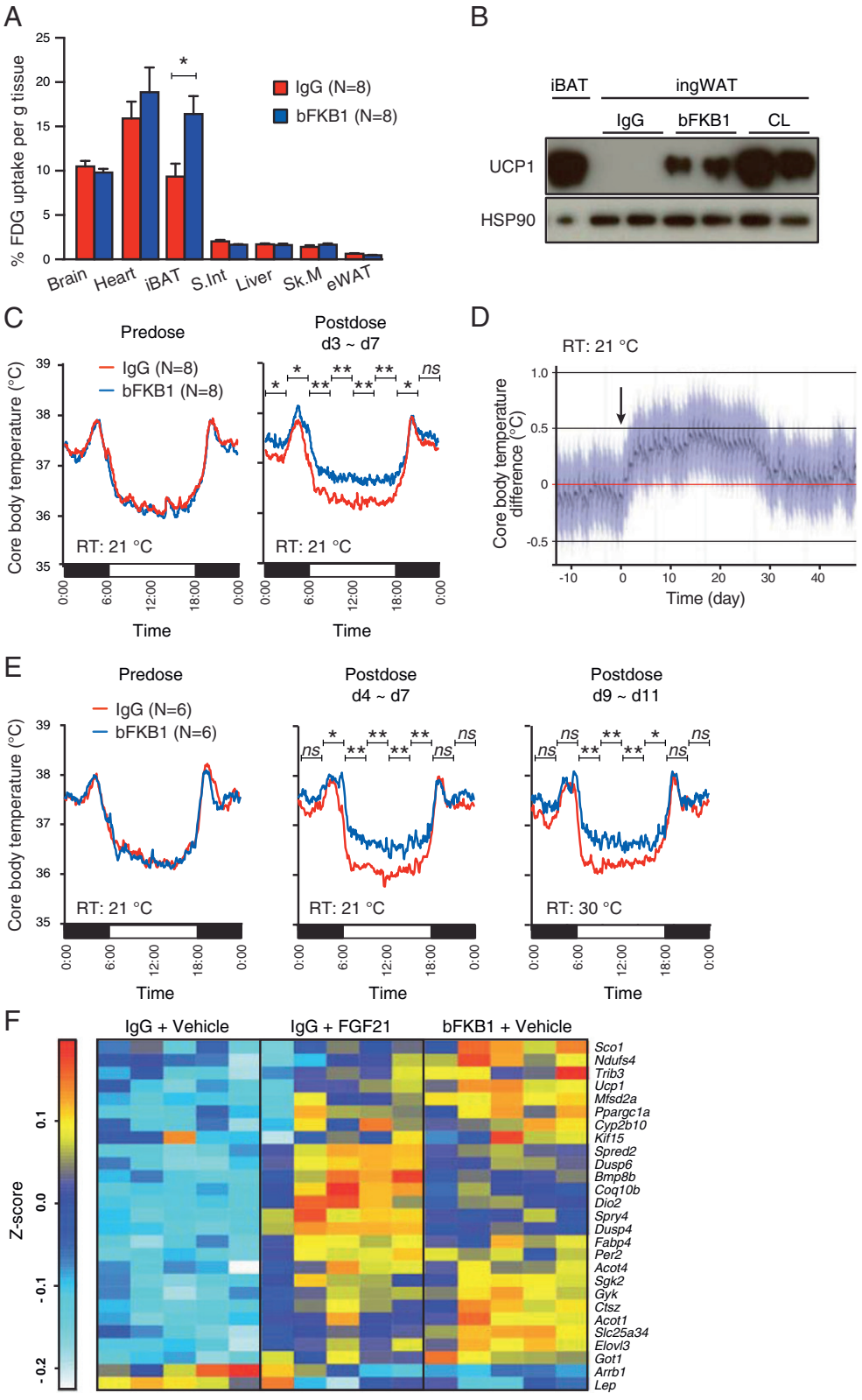

Fig. 5. BAT stimulation and WAT browning by bFKB1 (A) Tissue FDG-uptake in DIO mice at 40 h after single i.p. injection of indicated IgG at 10 mpk. Mice were fasted overnight before FDG-uptake measurement. Data is mean ± SEM and represents % of dose given, normalized by tissue weight. (B) Western blot analysis of ingWAT harvested on day 7 after single i.p. injection (bFKB1 or control IgG at 10 mpk) and surgical implantation of an osmotic pump (CL-316,243 at 0.75 nmol/h or vehicle). (C) Core body temperature measurement in DIO mice. Mice received 10 mpk of bFKB1 or control IgG. The data shown are the mean values of 5 days in predose and postdose periods. (D) The same experimental result in (C) was plotted to show the fitted difference in core body temperature between mice received bFKB1 or control IgG over the course of the study. The black line is the estimated difference and the blue lines are the 95% pointwise confidence intervals of the difference. IgG was administered on day 0 (arrow). (E) Core body temperature measurement in DIO mice. Mice received 10 mpk of bFKB1 or control IgG. Cage temperature was elevated to thermoneutrality on day 8 after the injection. The data shown are the mean values of 3–4 days in predose and postdose periods. Error bars omitted in (C) and (E) for clarity. $p < 0.05$ (*), <0.005 (**) vs control. (F) Gene expression profile in iBAT of DIO mice received single 10 mpk of IgG and hFGF21 b.i.d. at 2 mpk per day or vehicle PBS b.i.d. for 5 days. Tissue RNA was prepared on day 5 after the IgG injection. Of all the genes that were significantly altered by bFKB1 and hFGF21, only representative genes are listed. The results represent Z-score shown as a heat map and each column represents independent animal. N = 5 mice per group.

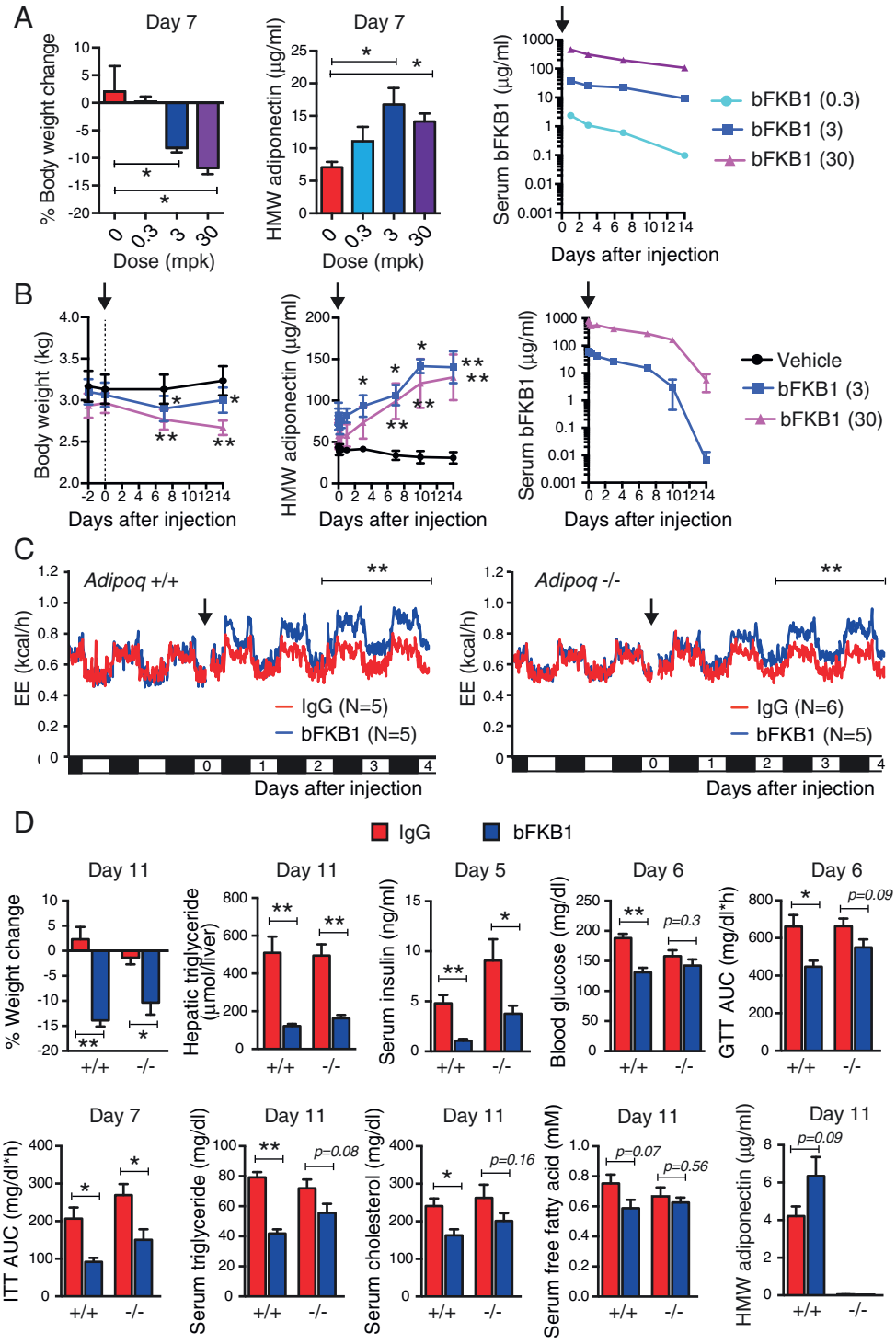

Fig. 6. Role of adiponectin in the bFKB1 treatment (A, B) Body weight change, serum HMW adiponectin and serum human bFKB1 levels in DIO mice ((A), N = 6 mice per group) or cynomolgus monkeys ((B), N = 3 monkeys per group) received single i.v. injection of bFKB1 at indicated dose (mpk). Pre-dose mean body weight ± SEM of mice used in (A) was 44.0 ± 1.3 (vehicle), 44.7 ± 1.2 (0.3 mpk), 46.5 ± 0.5 (3 mpk) and 42.1 ± 1.3 (30 mpk) g. (C) Mean EE values per mouse of DIO mice (left: WT and right: *Adipoq* KO) received single i.p. injection of indicated IgG at 10 mpk (arrow). Error bars omitted for clarity. (D) Metabolic parameters in WT (+/+) and *Adipoq* KO (−/−) DIO mice treated with single i.p. injection of indicated IgG at 10 mpk. Pre-dose mean body weight ± SEM was 47.5 ± 2.3 (WT, IgG), 47.6 ± 2.1 (WT, bFKB1), 47.3 ± 1.7 (KO, IgG) and 47.6 ± 1.6 (KO, bFKB1) g. N = 5–6 mice per group. AUC: area under the curve in GTT or ITT (T = 0–2 h). $p < 0.05$ (*), <0.005 (**) vs control. In (B), p values are calculated using % change from the base line. Data are mean ± SEM.

only FGFR1c. This difference translates into tissue selectivity; FGF21 activates MAPK signaling both in adipose tissues and the liver, and bFKB1 does not do so in the liver. Our work thus demonstrates that liver signaling is dispensable for FGF21-like effects in the context of robust adipose tissue effects. As a potential therapeutic molecule that has already been sequence-optimized for pharmaceutical properties, bFKB1 possesses unique advantages over previously described FGF21-analogs, including durability of the efficacy, receptor selectivity, and the lack of risk to induce cross-reactive antibodies against endogenous FGF21 protein.

One important consideration when designing an FGFR/KLB agonist molecule for a therapeutic purpose was to avoid interference of endogenous FGF signaling pathways. Previously, it was reported that an antibody-mediated inhibition of FGF/FGFR1 interaction (with anti-FGFR1) or FGF19/FGFR4 interaction (with anti-FGF19) caused severe

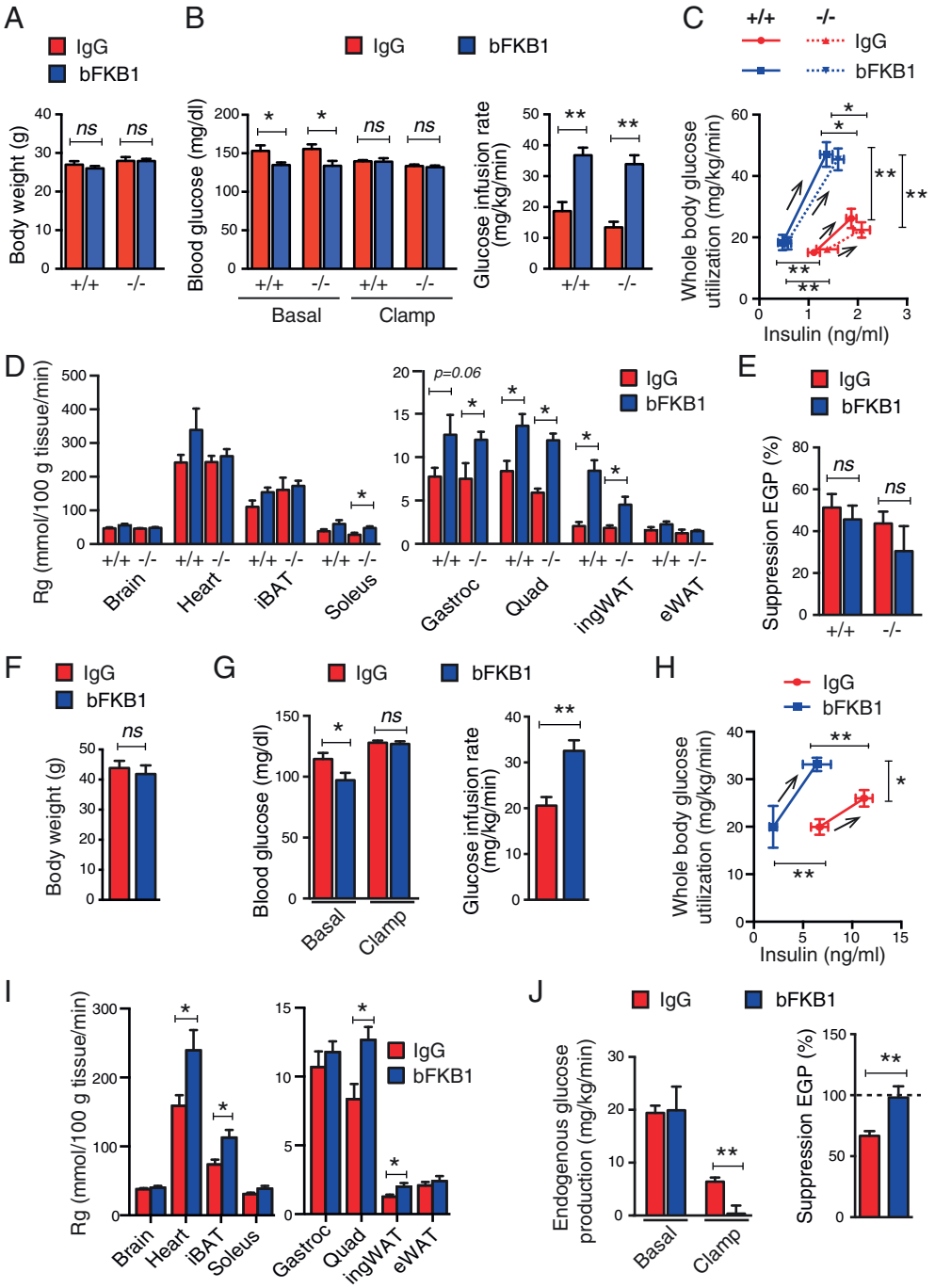

Fig. 7. Adiponectin-independent insulin sensitization by bFKB1 in hyperinsulinemic–euglycemic clamp (A) Body weight on the day of the clamp experiment. WT (+/+) and *Adipoq* KO (−/−) mice on HFD received bFKB1 or control IgG at 10 mpk on 3 days before the clamp experiment. N = 8–10 mice per group. (B) Arterial blood glucose at baseline and during the steady state (left) and glucose infusion rate during the steady state (right). (C) Whole body glucose utilization plotted against plasma insulin level. (D) Insulin-stimulated tissue glucose uptake. (E) % suppression of endogenous glucose production (EGP). (F) Body weight on the day of the second clamp experiment. DIO mice received bFKB1 or control IgG at 10 mpk on 5 days before the clamp experiment. N = 11–12 mice per group. (G) Arterial blood glucose at baseline and during the steady state (left) and glucose infusion rate during the steady state (right). (H) Whole body glucose utilization plotted against plasma insulin level. (I) Insulin-stimulated tissue glucose uptake. (J) EGP and % suppression. In (C) and (H), the arrows indicate the direction of changes from the basal to the insulin-stimulated state. $p < 0.05$ (*), <0.005 (**) vs control. Data are mean ± SEM.

weight loss in cynomolgus monkeys due to hypophagia and bile acid-mediated liver toxicity, respectively (Pai et al., 2012; Sun et al., 2007). In addition, FGFR1 inhibition has been implicated in phosphate dysregulation (Xiao et al., 2014; Yanochko et al., 2013). Therefore, we purposefully engineered a bispecific antibody by combining a high affinity anti-KLB antibody that does not compete with FGF21 or FGF19 for KLB binding, and an anti-FGFR1 antibody with a very weak affinity. As a consequence, our antibody lacks an ability to appreciably interfere with FGF19 signaling or phosphate homeostasis. In contrast, the previously described non-FGF-based high affinity FGFR1/KLB agonists exhibited the ability to block FGF–FGFR1 or FGF–KLB binding (Foltz et al., 2012; Smith et al., 2013) in vitro, and may compete with endogenous ligands for binding to their respective cognate receptors in vivo.

Although the mechanism of BAT stimulation and WAT browning by bFKB1 is not entirely clear, the onset of EE and core resting body temperature induction by bFKB1 and the gene expression signature in iBAT are consistent with a transcription-mediated mechanism. We have previously shown that the transcriptional factor cAMP

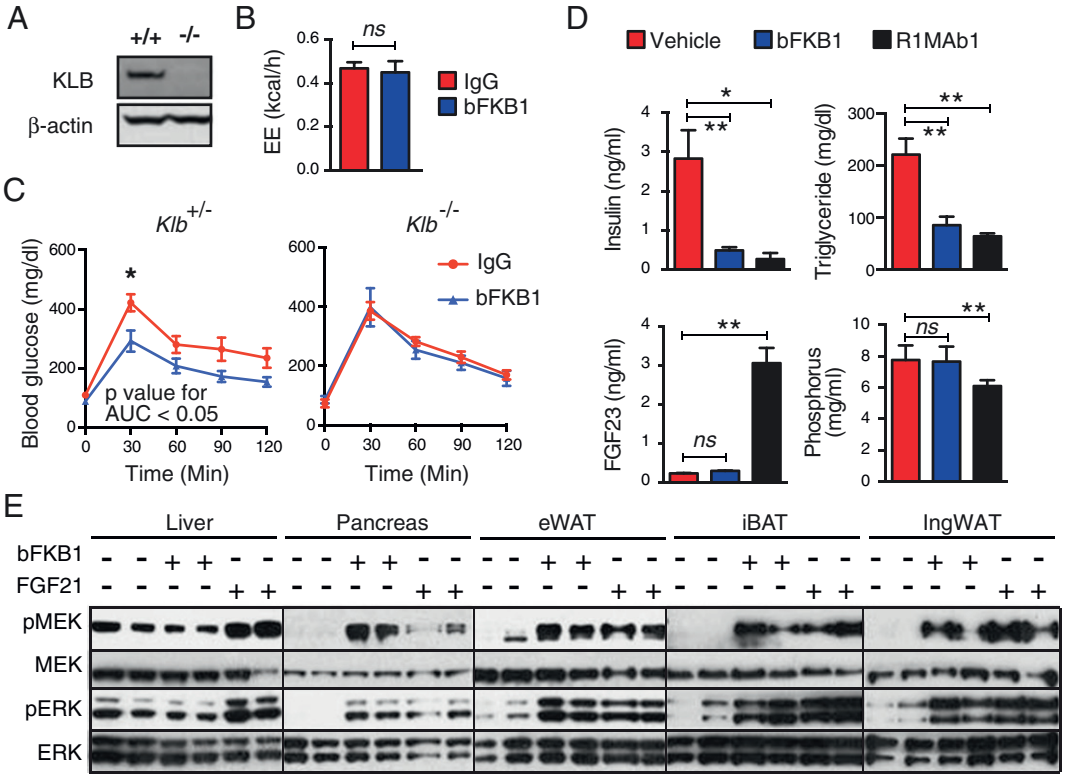

Fig. 8. Evidence for FGFR1- and KLB-dependent activity of bFKB1 in vivo. (A) Western blot analysis of epididymal WAT (eWAT) from WT (+/+) or *Klb*-deficient (−/−) mice. (B) Mean EE values per mouse during 4–5 days post IgG injection at 10 mpk in *Klb*-deficient DIO mice measured by indirect calorimetry. N = 6 mice per group. (C) GTT with DIO mice heterozygous (+/−) or homozygous (−/−) for the *Klb*-deficient allele. Mice received 4 weekly injections of bFKB1 or control IgG at 3 mpk. GTT was conducted on day 23, on 3 days after the final injection. N = 5 mice per group. (D) Serum parameters in DIO mice on day 7 after i.p. injection of bFKB1 or R1MAb1 at 50 mpk or vehicle. N = 6 mice per group. (E) MAPK signal activation by bFKB1 or hFGF21 in mouse tissues. Tissues were harvested at 1 h (liver, pancreas and eWAT) or 2 h (iBAT or ingWAT) after i.p. injection of lean mice at 10 mpk (bFKB1) or 1 mpk (FGF21). $p < 0.05$ (*), <0.01 (**). Data are mean ± SEM.

response element-binding protein (CREB) acts downstream of FGFR1 in adipocytes to induce *Ucp1* and *peroxisome proliferator-activated receptor gamma coactivator 1-alpha* (*PGC-1α*) gene expression (Wu et al., 2011a). Thus bFKB1 likely acts via CREB activation by directly acting on the FGFR1/KLB receptor expressed in adipocytes. This notion is supported by previous studies demonstrating that *Fgfr1* and *Klb* expressed in *aP2*-CRE expressing adipocytes are important for the pharmacological action of FGF21 (Adams et al., 2012; Ding et al., 2012; Foltz et al., 2012). Interestingly, the robust induction in EE by bFKB1 (or FGF21) administration could occur without an apparent change in RQ. Thus, unlike administration of sympathomimetics (norepinephrine, isoproterenol, or β_3-specific adrenoceptor agonist CL-316,243), cardiac natriuretic peptides, glp-1/glucagon coagonists, and interleukin-4 (Bordicchia et al., 2012; Day et al., 2009; Gavrilova et al., 2000; Nguyen et al., 2011), BAT stimulation through FGFR1/KLB complex can increases EE without altering the relative rate of fat and carbohydrate utilization. In this regard, the activation of FGFR1/KLB complex represents a unique pharmacological approach to selectively stimulate thermogenesis in BAT while avoiding indiscriminate activation of the sympathetic nervous system (SNS) and its potential toxicity (Dong et al., 2013; Yen and Ewald, 2012).

In addition to adipocytes, FGFR/KLB receptors expressed in the central nervous system (CNS) maybe important for the pharmacological stimulation of BAT activity by bFKB1. A recent report demonstrated that systemically injected FGF21 stimulates sympathetic nerves innervating iBAT (Owen et al., 2014). Furthermore, *Klb* in *Camk2a*-CRE expressing cells in CNS is essential for almost all FGF21 mediated pharmacological activity (Bookout et al., 2013; Owen et al., 2013, 2014). Thus, it is possible that the full action of bFKB1 requires both transcriptional activation in adipocytes and an independent stimulation of sympathetic nerves that innervate into BAT. While FGF21 can efficiently cross the blood–brain-barrier (Hsuchou et al., 2007), only 0.1–0.2% of circulating IgG is able to cross the blood–brain-barrier and reach the CNS (Yu et al., 2011). Currently, it is not clear whether a minute level of bFKB1 is sufficient to produce any brain signal. Defining the sites of action for bFKB1 would require testing its metabolic action in tissue-selective *Klb* and/or *Fgfr1* KO strains.

In addition to BAT stimulation, another important action of FGF21 is to increase adiponectin secretion from adipocytes, likely via a post-transcriptional mechanism (Gaich et al., 2013; Holland et al., 2013; Kharitonenkov et al., 2007; Lin et al., 2013). In fact, recently published studies demonstrate that FGF21 is efficacious in mice even in the absence of *Ucp1* gene (Samms et al., 2015; Véniant et al., 2015). In our study, activation of FGFR1/KLB complex alone led to a twofold increase in circulating HMW adiponectin in both mice and cynomolgus monkeys, demonstrating the central role of FGFR1/KLB complex in regulating HMW adiponectin levels. Numerous studies in the past 20 years support the critical role of adiponectin, in particular the HMW form of it, in improving insulin sensitivity and metabolic homeostasis through pleiotropic actions in multiple cell types (Kadowaki et al., 2014; Ye and Scherer, 2013). Indeed, we found that adiponectin deficiency in KO mice moderates the metabolic benefits of bFKB1 based on the examination of mice on 6 to 11 days after an antibody injection, consistent with the previous report with FGF21 (Holland et al., 2013; Lin et al., 2013). In addition, we also found that at an earlier time point, 3 days after an injection, the insulin sensitizing action of bFKB1 is intact in adiponectin deficient mice. Collectively, we propose that BAT stimulation plays the dominant role in the acute insulin sensitizing and lipid lowering effects of FGFR1/KLB activation in mice and adiponectin contributes at later time to enhance the amplitude of the metabolic benefits.

Although the list of anti-obesity and anti-diabetic agents is growing, a need for novel therapeutic agents to address obesity and type 2 diabetes clearly persists. The FGF21/19-class of therapeutic molecules provides us with the opportunity to explore the emerging concept of stimulating BAT activity and inducing WAT browning to combat human obesity and related diseases. Based on our findings, we envisage that antibody-mediated activation of FGFR1/KLB complex may enable more efficient and perhaps safer pharmacological intervention as opposed to the broad FGFR/KLB complex activation by FGF21 or FGF19 analogs.

Conflict of Interest

GK, MZC, RT, JZS, LK, NVB, JR, SKW, VDG, RADC, DRD, ALW, BH, KA, SW, XYR, NLK, YZ, JG, AB, TRG, DS, SR, TWB, JMV, YGM, JZ, RHS, MJB, YC, SS, HSK, LCA, EL, CS, YW, JAE, ASP, and JS are present or former paid employees of Genentech/Roche. OPW is a paid consultant for Genentech. Genentech has filed patent applications related to this work.

Acknowledgments

We thank Genentech colleagues for their technical assistance. We thank Drs. Bernard Allan and Chris Siebel for their critical reading of the draft manuscript. The glucose clamp experiments were conducted by the Vanderbilt Mouse Metabolic Phenotyping Center (DK059637) and Hormone Assay and Analytical Services Core (DK059637 and DK020593).

Appendix A. Supplementary Data

Supplemental Information includes five Supplemental Figures, Supplemental Materials and Methods, and Author Contributions. Supplementary data associated with this article can be found, in the online version, at http://dx.doi.org/10.1016/j.ebiom.2015.05.028.

References

Adams, A.C., Yang, C., Coskun, T., Cheng, C.C., Gimeno, R.E., Luo, Y., Kharitonenkov, A., 2012. The breadth of FGF21's metabolic actions are governed by FGFR1 in adipose tissue. Mol. Metab. 2, 31–37.

Ayala, J.E., Bracy, D.P., McGuinness, O.P., Wasserman, D.H., 2006. Considerations in the design of hyperinsulinemic–euglycemic clamps in the conscious mouse. Diabetes 55, 390–397.

Bookout, A.L., de Groot, M.H., Owen, B.M., Lee, S., Gautron, L., Lawrence, H.L., Ding, X., Elmquist, J.K., Takahashi, J.S., Mangelsdorf, D.J., et al., 2013. FGF21 regulates metabolism and circadian behavior by acting on the nervous system. Nat. Med. 19, 1147–1152.

Bordicchia, M., Liu, D., Amri, E.Z., Ailhaud, G., Dessi-Fulgheri, P., Zhang, C., Takahashi, N., Sarzani, R., Collins, S., 2012. Cardiac natriuretic peptides act via p38 MAPK to induce the brown fat thermogenic program in mouse and human adipocytes. J. Clin. Invest. 122, 1022–1036.

Cannon, B., Nedergaard, J., 2004. Brown adipose tissue: function and physiological significance. Physiol. Rev. 84, 277–359.

Chan, A.C., Carter, P.J., 2010. Therapeutic antibodies for autoimmunity and inflammation. Nat. Rev. Immunol. 10, 301–316.

Coskun, T., Bina, H.A., Schneider, M.A., Dunbar, J.D., Hu, C.C., Chen, Y., Moller, D.E., Kharitonenkov, A., 2008. Fibroblast growth factor 21 corrects obesity in mice. Endocrinology 149, 6018–6027.

Cypess, A.M., Weiner, L.S., Roberts-Toler, C., Elia, E.F., Kessler, S.H., Kahn, P.A., English, J., Chatman, K., Trauger, S.A., Doria, A., et al., 2015. Activation of human brown adipose tissue by a beta3-adrenergic receptor agonist. Cell Metab. 21, 33–38.

Day, J.W., Ottaway, N., Patterson, J.T., Gelfanov, V., Smiley, D., Gidda, J., Findeisen, H., Bruemmer, D., Drucker, D.J., Chaudhary, N., et al., 2009. A new glucagon and GLP-1 co-agonist eliminates obesity in rodents. Nat. Chem. Biol. 5, 749–757.

Ding, X., Boney-Montoya, J., Owen, B.M., Bookout, A.L., Coate, K.C., Mangelsdorf, D.J., Kliewer, S.A., 2012. betaKlotho is required for fibroblast growth factor 21 effects on growth and metabolism. Cell Metab. 16, 387–393.

Dong, M., Yang, X., Lim, S., Cao, Z., Honek, J., Lu, H., Zhang, C., Seki, T., Hosaka, K., Wahlberg, E., et al., 2013. Cold exposure promotes atherosclerotic plaque growth and instability via UCP1-dependent lipolysis. Cell Metab. 18, 118–129.

Fisher, F.M., Kleiner, S., Douris, N., Fox, E.C., Mepani, R.J., Verdeguer, F., Wu, J., Kharitonenkov, A., Flier, J.S., Maratos-Flier, E., et al., 2012. FGF21 regulates PGC-1α and browning of white adipose tissues in adaptive thermogenesis. Genes Dev. 26, 271–281.

Foltz, I.N., Hu, S., King, C., Wu, X., Yang, C., Wang, W., Weiszmann, J., Stevens, J., Chen, J.S., Nuanmanee, N., et al., 2012. Treating diabetes and obesity with an FGF21-mimetic antibody activating the betaKlotho/FGFR1c receptor complex. Sci. Transl. Med. 4, 162ra153.

Fon Tacer, K., Bookout, A.L., Ding, X., Kurosu, H., John, G.B., Wang, L., Goetz, R., Mohammadi, M., Kuro-o, M., Mangelsdorf, D.J., et al., 2010. Research resource: comprehensive expression atlas of the fibroblast growth factor system in adult mouse. Mol. Endocrinol. 24, 2050–2064.

French, D.M., Lin, B.C., Wang, M., Adams, C., Shek, T., Hotzel, K., Bolon, B., Ferrando, R., Blackmore, C., Schroeder, K., et al., 2012. Targeting FGFR4 inhibits hepatocellular carcinoma in preclinical mouse models. PLoS One 7, e36713.

Friedman, B.A., Maniatis, T., 2011. ExpressionPlot: a web-based framework for analysis of RNA-Seq and microarray gene expression data. Genome Biol. 12, R69.

Frontini, A., Vitali, A., Perugini, J., Murano, I., Romiti, C., Ricquier, D., Guerrieri, M., Cinti, S., 2013. White-to-brown transdifferentiation of omental adipocytes in patients affected by pheochromocytoma. Biochim. Biophys. Acta 1831, 950–959.

Fu, L., John, L.M., Adams, S.H., Yu, X.X., Tomlinson, E., Renz, M., Williams, P.M., Soriano, R., Corpuz, R., Moffat, B., et al., 2004. Fibroblast growth factor 19 increases metabolic rate and reverses dietary and leptin-deficient diabetes. Endocrinology 145, 2594–2603.

Gaich, G., Chien, J.Y., Fu, H., Glass, L.C., Deeg, M.A., Holland, W.L., Kharitonenkov, A., Bumol, T., Schilske, H.K., Moller, D.E., 2013. The effects of LY2405319, an FGF21 analog, in obese human subjects with type 2 diabetes. Cell Metab. 18, 333–340.

Gavrilova, O., Marcus-Samuels, B., Reitman, M.L., 2000. Lack of responses to a beta3-adrenergic agonist in lipoatrophic A-ZIP/F-1 mice. Diabetes 49, 1910–1916.

Holland, W.L., Adams, A.C., Brozinick, J.T., Bui, H.H., Miyauchi, Y., Kusminski, C.M., Bauer, S.M., Wade, M., Singhal, E., Cheng, C.C., et al., 2013. An FGF21–adiponectin–ceramide axis controls energy expenditure and insulin action in mice. Cell Metab. 17, 790–797.

Hsuchou, H., Pan, W., Kastin, A.J., 2007. The fasting polypeptide FGF21 can enter brain from blood. Peptides 28, 2382–2386.

Inagaki, T., Lin, V.Y., Goetz, R., Mohammadi, M., Mangelsdorf, D.J., Kliewer, S.A., 2008. Inhibition of growth hormone signaling by the fasting-induced hormone FGF21. Cell Metab. 8, 77–83.

Kadowaki, T., Yamauchi, T., Okada-Iwabu, M., Iwabu, M., 2014. Adiponectin and its receptors: implications for obesity-associated diseases and longevity. Lancet Diabetes Endocrinol. 2, 8–9.

Kharitonenkov, A., Wroblewski, V.J., Koester, A., Chen, Y.-F., Clutinger, C.K., Tigno, X.T., Hansen, B.C., Shanafelt, A.B., Etgen, G.J., 2007. The metabolic state of diabetic monkeys is regulated by fibroblast growth factor-21. Endocrinology 148, 774–781.

Kurosu, H., Choi, M., Ogawa, Y., Dickson, A.S., Goetz, R., Eliseenkova, A.V., Mohammadi, M., Rosenblatt, K.P., Kliewer, S.A., Kuro-o, M., 2007. Tissue-specific expression of betaKlotho and fibroblast growth factor (FGF) receptor isoforms determines metabolic activity of FGF19 and FGF21. J. Biol. Chem. 282, 26687–26695.

Lin, Z., Tian, H., Lam, K.S., Lin, S., Hoo, R.C., Konishi, M., Itoh, N., Wang, Y., Bornstein, S.R., Xu, A., et al., 2013. Adiponectin mediates the metabolic effects of FGF21 on glucose homeostasis and insulin sensitivity in mice. Cell Metab. 17, 779–789.

Micanovic, R., Raches, D.W., Dunbar, J.D., Driver, D.A., Bina, H.A., Dickinson, C.D., Kharitonenkov, A., 2009. Different roles of N- and C-termini in the functional activity of FGF21. J. Cell. Physiol. 219, 227–234.

Nedergaard, J., Bengtsson, T., Cannon, B., 2007. Unexpected evidence for active brown adipose tissue in adult humans. Am. J. Physiol. Endocrinol. Metab. 293, E444–E452.

Ng, M., Fleming, T., Robinson, M., Thomson, B., Graetz, N., Margono, C., Mullany, E.C., Biryukov, S., Abbafati, C., Abera, S.F., et al., 2014. Global, regional, and national prevalence of overweight and obesity in children and adults during 1980–2013: a systematic analysis for the Global Burden of Disease Study 2013. Lancet 384, 766–781.

Nguyen, K.D., Qiu, Y., Cui, X., Goh, Y.P., Mwangi, J., David, T., Mukundan, L., Brombacher, F., Locksley, R.M., Chawla, A., 2011. Alternatively activated macrophages produce catecholamines to sustain adaptive thermogenesis. Nature 480, 104–108.

Owen, B.M., Bookout, A.L., Ding, X., Lin, V.Y., Atkin, S.D., Gautron, L., Kliewer, S.A., Mangelsdorf, D.J., 2013. FGF21 contributes to neuroendocrine control of female reproduction. Nat. Med. 19, 1153–1156.

Owen, B.M., Ding, X., Morgan, D.A., Coate, K.C., Bookout, A.L., Rahmouni, K., Kliewer, S.A., Mangelsdorf, D.J., 2014. FGF21 Acts Centrally to Induce Sympathetic Nerve Activity, Energy Expenditure, and Weight Loss. Cell Metab. 20, 670–677.

Pai, R., French, D., Ma, N., Hotzel, K., Plise, E., Salphati, L., Setchell, K.D.R., Ware, J., Lauriault, V., Schutt, L., et al., 2012. Antibody-mediated inhibition of fibroblast growth factor 19 results in increased bile acids synthesis and ileal malabsorption of bile acids in cynomolgus monkeys. Toxicol. Sci. 126, 446–456.

Samms, R.J., Smith, D.P., Cheng, C.C., Antonellis, P.P., Perfield, J.W., 2nd, Kharitonenkov, A., Gimeno, R.E., Adams, A.C., 2015. Discrete aspects of FGF21 in vivo pharmacology do not require UCP1. Cell Rep. 11, 991–999.

Shatz, W., Chung, S., Li, B., Marshall, B., Tejada, M., Phung, W., Sandoval, W., Kelley, R.F., Scheer, J.M., 2013. Knobs-into-holes antibody production in mammalian cell lines reveals that asymmetric afucosylation is sufficient for full antibody-dependent cellular cytotoxicity. MAbs 5, 872–881.

Shulman, G.I., 2014. Ectopic fat in insulin resistance, dyslipidemia, and cardiometabolic disease. N. Engl. J. Med. 371, 1131–1141.

Sidossis, L., Kajimura, S., 2015. Brown and beige fat in humans: thermogenic adipocytes that control energy and glucose homeostasis. J. Clin. Invest. 125, 478–486.

Smith, R., Duguay, A., Bakker, A., Li, P., Weiszmann, J., Thomas, M.R., Alba, B.M., Wu, X., Gupte, J., Yang, L., et al., 2013. FGF21 can be mimicked in vitro and in vivo by a novel anti-FGFR1c/beta-Klotho bispecific protein. PLoS One 8, e61432.

Sondergaard, E., Gormsen, L.C., Christensen, M.H., Pedersen, S.B., Christiansen, P., Nielsen, S., Poulsen, P.L., Jessen, N., 2015. Chronic adrenergic stimulation induces brown adipose tissue differentiation in visceral adipose tissue. Diabet. Med. 32, e4–e8.

Spiess, C., Merchant, M., Huang, A., Zheng, Z., Yang, N.Y., Peng, J., Ellerman, D., Shatz, W., Reilly, D., Yansura, D.G., et al., 2013. Bispecific antibodies with natural architecture

produced by co-culture of bacteria expressing two distinct half-antibodies. Nat. Biotechnol. 31, 753–758.
Sun, H.D., Malabunga, M., Tonra, J.R., DiRenzo, R., Carrick, F.E., Zheng, H., Berthoud, H.-R., McGuinness, O.P., Shen, J., Bohlen, P., et al., 2007. Monoclonal antibody antagonists of hypothalamic FGFR1 cause potent but reversible hypophagia and weight loss in rodents and monkeys. Am. J. Physiol. Endocrinol. Metab. 292, E964–E976.
Tomlinson, E., Fu, L., John, L., Hultgren, B., Huang, X., Renz, M., Stephan, J.P., Tsai, S.P., Powell-Braxton, L., French, D., et al., 2002. Transgenic mice expressing human fibroblast growth factor-19 display increased metabolic rate and decreased adiposity. Endocrinology 143, 1741–1747.
Véniant, M.M., Sivits, G., Helmering, J., Komorowski, R., Lee, J., Fan, W., Moyer, C., Lloyd, D.J., 2015. Pharmacologic effects of FGF21 are independent of the "browning" of white adipose tissue. Cell Metab. 21, 731–738.
Wei, W., Dutchak, P.A., Wang, X., Ding, X., Wang, X., Bookout, A.L., Goetz, R., Mohammadi, M., Gerard, R.D., Dechow, P.C., et al., 2012. Fibroblast growth factor 21 promotes bone loss by potentiating the effects of peroxisome proliferator-activated receptor gamma. Proc. Natl. Acad. Sci. U. S. A. 109, 3143–3148.
Wu, A.-L., Coulter, S., Liddle, C., Wong, A., Eastham-Anderson, J., French, D.M., Peterson, A.S., Sonoda, J., 2011a. FGF19 regulates cell proliferation, glucose and bile acid metabolism via FGFR4-dependent and independent pathways. PLoS ONE 6, e17868.
Wu, A.L., Kolumam, G., Stawicki, S., Chen, Y., Li, J., Zavala-Solorio, J., Phamluong, K., Feng, B., Li, L., Marsters, S., et al., 2011b. Amelioration of type 2 diabetes by antibody-mediated activation of fibroblast growth factor receptor 1. Sci. Transl. Med. 3, 113ra126.
Wu, A.L., Feng, B., Chen, M.Z., Kolumam, G., Zavala-Solorio, J., Wyatt, S.K., Gandham, V.D., Carano, R.A., Sonoda, J., 2013. Antibody-mediated activation of FGFR1 induces FGF23 production and hypophosphatemia. PLoS One 8, e57322.
Xiao, Z., Huang, J., Cao, L., Liang, Y., Han, X., Quarles, L.D., 2014. Osteocyte-specific deletion of Fgfr1 suppresses FGF23. PLoS One 9, e104154.
Xu, J., Lloyd, D.J., Hale, C., Stanislaus, S., Chen, M., Sivits, G., Vonderfecht, S., Hecht, R., Li, Y., Lindberg, R.A., et al., 2009. Fibroblast growth factor 21 reverses hepatic steatosis, increases energy expenditure, and improves insulin sensitivity in diet-induced obese mice. Diabetes 58, 250–259.
Yanochko, G.M., Vitsky, A., Heyen, J.R., Hirakawa, B., Lam, J.L., May, J., Nichols, T., Sace, F., Trajkovic, D., Blasi, E., 2013. Pan-FGFR inhibition leads to blockade of FGF23 signaling, soft tissue mineralization, and cardiovascular dysfunction. Toxicol. Sci. 135, 451–464.
Ye, R., Scherer, P.E., 2013. Adiponectin, driver or passenger on the road to insulin sensitivity? Mol. Metab. 2, 133–141.
Yen, M., Ewald, M.B., 2012. Toxicity of weight loss agents. J. Med. Toxicol. 8, 145–152.
Yie, J., Hecht, R., Patel, J., Stevens, J., Wang, W., Hawkins, N., Steavenson, S., Smith, S., Winters, D., Fisher, S., et al., 2009. FGF21 N- and C-termini play different roles in receptor interaction and activation. FEBS Lett. 583, 19–24.
Yie, J., Wang, W., Deng, L., Tam, L.-T., Stevens, J., Chen, M.M., Li, Y., Xu, J., Lindberg, R., Hecht, R., et al., 2012. Understanding the physical interactions in the FGF21/FGFR/β-Klotho complex: structural requirements and implications in FGF21 signaling. Chem. Biol. Drug Des. 79, 398–410.
Yoneshiro, T., Aita, S., Matsushita, M., Kayahara, T., Kameya, T., Kawai, Y., Iwanaga, T., Saito, M., 2013. Recruited brown adipose tissue as an antiobesity agent in humans. J. Clin. Invest. 123, 3404–3408.
Yu, Y.J., Zhang, Y., Kenrick, M., Hoyte, K., Luk, W., Lu, Y., Atwal, J., Elliott, J.M., Prabhu, S., Watts, R.J., et al., 2011. Boosting brain uptake of a therapeutic antibody by reducing its affinity for a transcytosis target. Sci. Transl. Med. 3, 84ra44.